Chemistry–A European Journal
Research Article
doi.org/10.1002/chem.202300934
Chemistry Europe
European Chemical Societies Publishing
www.chemeurj.org

Electronic and Charge Transport Properties in Bridged versus Unbridged Nanohoops: Role of the Nanohoop Size

Fabien Lucas[+],[a] Clément Brouillac[+],[a] Nemo McIntosh,[b] Samuele Giannini,[b] Joëlle Rault-Berthelot,[a] Christophe Lebreton,[c] David Beljonne,[b] Jérôme Cornil,[b] Emmanuel Jacques,[c] Cassandre Quinton,[a] and Cyril Poriel*[a]

Abstract: In the field of π-conjugated nanohoops, the size of the macrocycle has a strong impact on its structural characteristics, which in turn affect its electronic properties. In this work, we report the first experimental investigations linking the size of a nanohoop to its charge transport properties, a key property in organic electronics. We describe the synthesis and study of the first example of a cyclocarbazole possessing five constituting building units, namely [5]-cyclo-*N*-butyl-2,7-carbazole, **[5]C-Bu-Cbz**. By comparison with a shorter analogue, [4]-cyclo-*N*-butyl-2,7-carbazole, **[4]C-Bu-Cbz**, we detail the photophysical, electrochemical, morphological and charge transport properties, highlighting the key role played by the hoop size. In particular, we show that the saturated field effect mobility of **[5]C-Bu-Cbz** is four times higher than that of its smaller analogue **[4]C-Bu-Cbz** (4.22×10^{-5} vs 1.04×10^{-5} $cm^2V^{-1}s^{-1}$). However, the study of the other organic field-effect transistor characteristics (threshold voltage V_{TH} and subthreshold slope SS) suggest that a small nanohoop is beneficial for good organization of the molecules in thin films, whereas a large one increases the density of structural defects, and hence of traps for the charge carriers. The present findings are of interest for the further development of nanohoops in electronics.

Introduction

π-Conjugated materials are at the heart of organic electronic devices such as organic light-emitting diodes (OLED), organic field-effect transistors (OFET) and organic photovoltaics (OPV).[1,2] The fantastic development of this technology undoubtedly arises from the development of precise molecular design tactics, which have allowed a perfect fit between a molecular/material property and a specific characteristic of an electronic device. The development of new molecular fragments and of new families of organic semiconductors is undoubtedly the strategy, which has allowed for the most important breakthroughs. The development of fullerenes is surely one of the nicest example to illustrate this feature.[3–6] In 2008, a new generation of π-conjugated systems, namely molecular nanohoops, has appeared in the literature.[7] Nanohoops belong to the family of curved π-systems, and have attracted a considerable attention worldwide due to their uncommon electronic properties arising from the radially distributed π-conjugation.[8–13] However, their incorporations in organic electronic devices remain poorly developed,[14–16] surely due to the difficulty to reach decent amount of materials for device fabrication. However, in recent years, the first experimental data on the charge transport of nanohoops have been reported[16–19] and have revealed, coupled to theoretical insights,[18,20–22] the potential of nanohoops. Used as host in red emitting phosphorescent OLED, nanohoops have also recently shown very promising results, being more efficient than their linear counterparts (external quantum efficiency of 17 vs 11%).[23]

Charge transport in organic semi-conductors is a central notion in organic electronics,[24] which drives the performance of the three principal devices, OLED, OFET and OPV. Investigating the charge transport of nanohoops is therefore an important step in their development.

The first measurement of nanohoop mobility was reported in 2017 by Yamago and co-workers.[16] A low electron mobility value of 5×10^{-6} $cm^2V^{-1}s^{-1}$ was measured in an electron-only device using the space-charge-limited current (SCLC) technique. In 2021, the first detailed structure-properties-device performances relationship study of functional materials based on nanohoops has shown how the nanohoop supramolecular arrangement can affect the corresponding OFET characteristics.[18] FE mobility values of approximately 10^{-5} $cm^2V^{-1}s^{-1}$ were measured with interesting OFET character-

[a] Dr. F. Lucas,[+] C. Brouillac,[+] Dr. J. Rault-Berthelot, Dr. C. Quinton, Dr. C. Poriel
Univ Rennes, CNRS, ISCR-UMR 6226
35000 Rennes (France)
E-mail: cyril.poriel@univ-rennes1.fr
[b] N. McIntosh, Dr. S. Giannini, Dr. D. Beljonne, Dr. J. Cornil
Laboratory for Chemistry of Novel Materials
University of Mons, Mons (Belgium)
[c] C. Lebreton, Dr. E. Jacques
Univ Rennes, CNRS, IETR-UMR 6164
35000 Rennes (France)
[+] These authors contributed equally to this manuscript.

Supporting information for this article is available on the WWW under https://doi.org/10.1002/chem.202300934

istics (low V_{TH}, low SS, high stability under electrical stress). The recent molecular design works performed by Du and co-workers have allowed to reach an electron mobility (SCLC) of 2×10^{-4} $cm^2V^{-1}s^{-1}$, which is the highest value reported so far in the field.[19] These first data have shown that functional nanohoops can be used as semi-conductors. However, defining the link between molecular structure and charge transport properties is one of the next barriers to lift in the field. In nanohoop chemistry, the electronic properties are driven by both the nature of the building units and by the hoop size; in the last five years, an increasing number of reports has been published on the subject.[25–32] However, as far as we know, there is no report on the experimental assessment of the influence on charge transport of the nanohoop size. In 2019, it has been shown that theoretical mobility of CPPs correlates with its hoop size and was mainly controlled by the reorganization energy.[33] This theoretical study has undoubtedly inspires the present work. Through two examples of size expansion (Scheme 1), we report herein the first experimental evidence on the link between the size and the charge transport in nanohoops.

The two couples studied in the purpose of this work are: [10]-cyclo-*para*-phenylene **[10]CPP** versus [8]-cyclo-*para*-phenylene **[8]CPP** and [5]-cyclo-*N*-butyl-2,7-carbazole **[5]C-Bu-Cbz** versus [4]-cyclo-*N*-butyl-2,7-carbazole **[4]C-Bu-Cbz**. They possess either 10 (**[10]CPP** and **[5]C-Bu-Cbz**) or 8 (**[8]CPP** and **[4]C-Bu-Cbz**) phenyl units, bridged, two by two, by a nitrogen atom in the case of cyclocarbazoles and unbridged in the case of CPPs. Bridges effects are an important concept in organic electronics, widely described for linear π-conjugated systems.[34–38] For nanohoops, the impact of the bridges on the electronic properties has also started to be investigated.[18,39] Note that this work also reports the first example of a [5]-cyclocarbazole nanohoop possessing five units, **[5]C-Bu-Cbz**. The whole study includes electrochemical, photophysical (in solution and in thin film), morphological and charge transport investigations and is coupled to theoretical calculations. We notably show that the saturated FE mobility of **[5]C-Bu-Cbz** is four times higher than that of its smaller analogue **[4]C-Bu-Cbz** (4.22×10^{-5} vs 1.04×10^{-5} $cm^2V^{-1}s^{-1}$). However, study of the other OFET parameters (threshold voltage V_{TH}, subthreshold slope SS) suggests that a small nanohoop is beneficial for a good organization of the molecules in thin films whereas a large one increases the density of structural defects, and hence of traps for the charge carriers. In addition, we show for both nanohoop families that when the size decreases, the charge carrier mobility (SCLC) increases (2.78×10^{-4} $cm^2V^{-1}s^{-1}$ for **[4]C-Bu-Cbz** vs 7.75×10^{-5} $cm^2V^{-1}s^{-1}$ for **[5]C-Bu-Cbz** and 1.21×10^{-7} $cm^2V^{-1}s^{-1}$ for **[8]CPP** vs 1.1×10^{-8} $cm^2V^{-1}s^{-1}$ for **[10]CPP**).

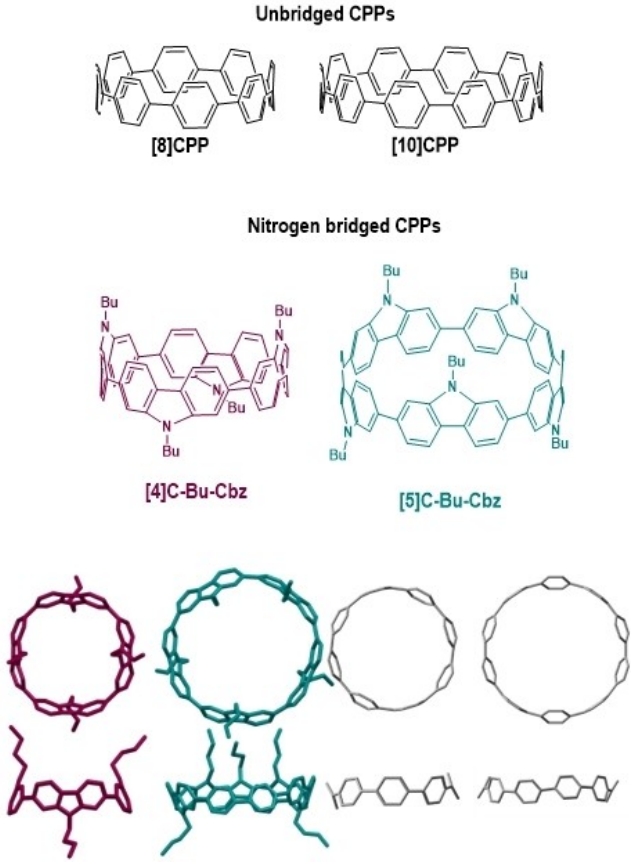

Scheme 1. Cyclocarbazoles with four (**[4]C-Bu-Cbz**) or five (**[5]C-Bu-Cbz**) carbazole units and their corresponding cyclo-*para*-phenylene analogues (**[8]CPP** and **[10]CPP**). Molecular structures obtained from DFT (B3LYP/6-31 g(d,p)).

Results and Discussion

Both **[4]C-Bu-Cbz** and **[5]C-Bu-Cbz** were synthesized by following the Pt approach initially developed by Yamago and co-workers in 2010[40] (Figure 1, top). First, the nitrogen atom of 2,7-dibromocarbazole was alkylated with a butyl chain and then functionalized with pinacolato boron units to give **1** (Chart S1 in the Supporting Information). The cyclization step follows an optimized procedure previously reported.[17] The intermediates **2** and **3**, based on four and five square-shaped platinum complexes, were formed (not isolated) by stirring the bispinacolato diboron carbazole **1** with $Pt(COD)Cl_2$ and cesium fluoride at 70 °C in 1,2-dichloroethane (DCE) for 24 h. Then, the carefully dried crude mixture containing both **2** and **3** was treated with triphenylphosphine in *ortho*-dichlorobenzene, 1 h at room temperature (RT) and 48 h at 180 °C to provide **[4]C-Bu-Cbz** and **[5]C-Bu-Cbz** with 58 and 2% yield, respectively. Despite **[5]C-Bu-Cbz** has been obtained with a low yield, the formation of a nanohoop with five constituting units appears very interesting to increase the molecular diversity of nanohoops. Indeed, this synthetic approach allows the formation of two nanohoop sizes, which is undoubtedly an interesting synthetic feature in the field, especially if an electronic application is targeted.[41–44]

In ^1H NMR, when increasing the size of the nanohoop (from **[4]C-Bu-Cbz** to **[5]C-Bu-Cbz**) and hence its number of building units, all signals are deshielded, especially Hc (Figure 1 bottom-left). This is assigned to the ring current[45,46] and the magnetic shielding effect, which is increased when the size of the nanohoop decreases.[9,47] The most shifted signal is observed for H_C, which is detected at 6.98 ppm for **[5]C-Bu-Cbz** and at

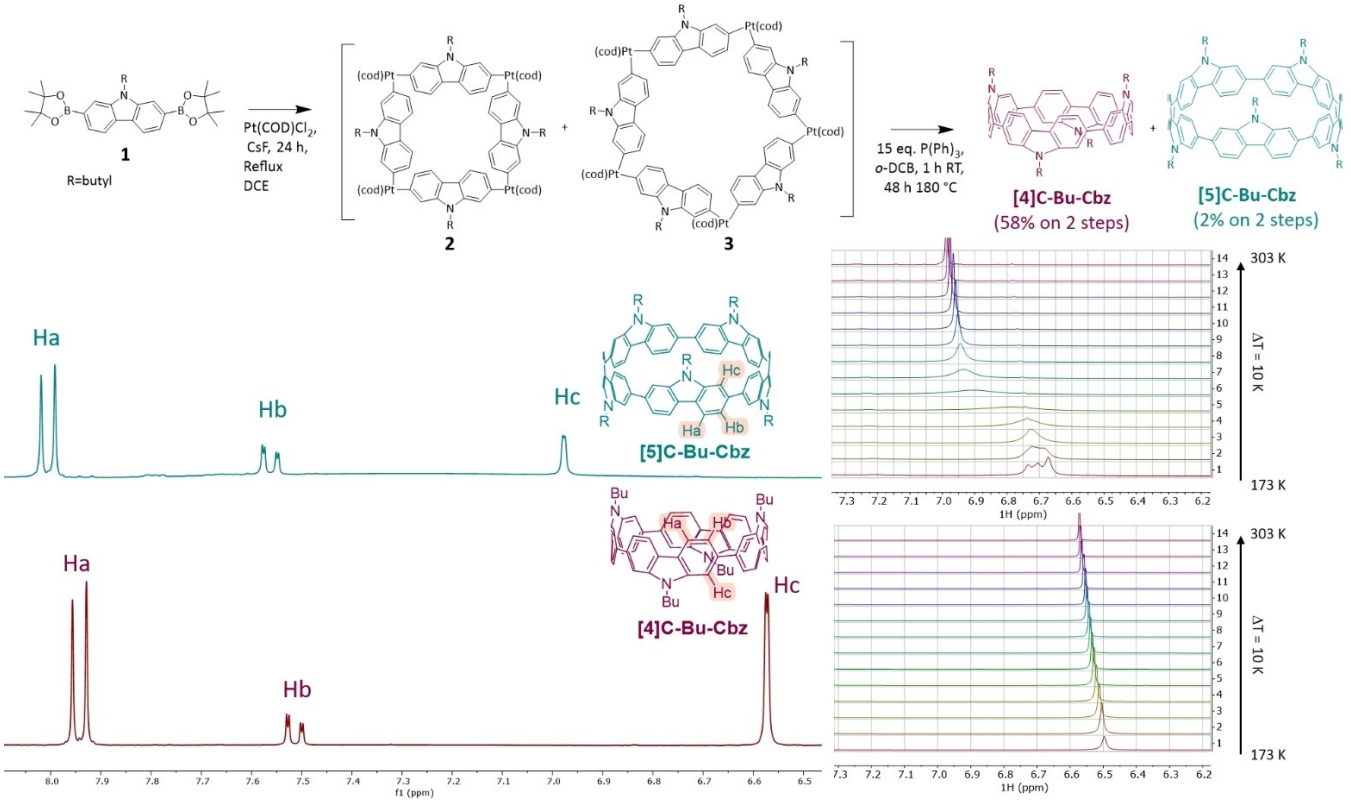

Figure 1. Top: Synthesis of **[4]C-Bu-Cbz** and **[5]C-Bu-Cbz**. Bottom: left: parts of the ^{1}H NMR spectra of **[5]C-Bu-Cbz** and **[4]C-Bu-Cbz** in CD_2Cl_2 (full spectra in Figures S1 and S2); right: zoom in on the Hc signal of the ^{1}H NMR spectrum as a function of the temperature of **[5]C-Bu-Cbz** (upper) and **[4]C-Bu-Cbz** (lower) in CD_2Cl_2 (full spectra in Figures S8–S11).

6.57 ppm for **[4]C-Bu-Cbz**. The main difference between **[5]C-Bu-Cbz** and **[4]C-Bu-Cbz** is their dynamics in solution. It has been previously shown in the case of nitrogen or carbon bridged cycloparaphenylenes with four building units (such as **[4]C-Bu-Cbz**) that a single conformer with an αβαβ orientation (i.e., with the bridges alternatively pointing up and down) is obtained.[17,48] In the case of **[5]C-Bu-Cbz**, variable temperature NMR studies indicate that a time-averaged dynamic structure is detected at room temperature, Figure 1 bottom-right. Indeed, if increasing the temperature up to 373 K does not modify the ^{1}H NMR spectrum (Figure S10), decreasing the temperature yields a very different behaviour. Hc illustrates well this behaviour. Indeed, from 303 to 173 K, the Hc signals become broader before splitting, after coalescence, in several signals at 173 K, which correspond to the different conformers of **[5]-Bu-Cbz** (Figure 1, bottom right, and Figure S8). The same experiment performed with **[4]C-Bu-Cbz** does not show any modification, thus indicating that a single conformer exists at room temperature (Figure 1, bottom right, and Figure S11). This shows the importance of the number of constituting units, that is, the size of the nanohoop, and the resulting strain on the dynamics of nanohoops in solution.[49] This is confirmed by the theoretical estimation of the strain energy, which is higher for **[4]C-Bu-Cbz** than for **[5]C-Bu-Cbz** (72 and 56 kcal mol^{-1}, respectively), see the Supporting Information for details of the calculation.

Electrochemical analyses of **[5]C-Bu-Cbz** were performed by cyclic voltammetry (CV) in CH_2Cl_2 for the oxidation and in DMF for the reduction (Figures S12–S15) and compared with **[10]CPP** and with **[4]C-Bu-Cbz** in order to respectively shed light on the impact of the bridging and of the nanohoop size. In oxidation, **[5]C-Bu-Cbz** displays an electrochemical behaviour reflecting an electrodeposition process occurring at the first oxidation wave, around 1.14 V vs SCE. The deposit growth is evidenced by the reduction detected at the reverse scan and by the regular increase of its redox wave when recording recurrent cycles (for a detailed study of the electrodeposition processes, see Figure S13). The deposit is oxidized at a lower anodic value than **[5]C-Bu-Cbz**. From the onset of the first wave, the HOMO energy level is evaluated at −5.22 eV for **[5]C-Bu-Cbz**, slightly below that of **[4]C-Bu-Cbz** (HOMO: −5.18 eV). Similarly, the LUMO energy of **[5]C-Bu-Cbz**, evaluated at −2.51 eV, is deeper than that of **[4]C-Bu-Cbz** (−2.40 eV). Thus, as the size of the cyclocarbazole increases from 4 to 5 units, there is a decrease of both HOMO and LUMO energies. Because the LUMO decrease (0.11 eV) is larger than the HOMO decrease (0.04 eV), there is a gap contraction of 0.07 eV when the number of carbazole units increases (from 2.78 eV in **[4]C-Bu-Cbz** to 2.71 eV in **[5]C-Bu-Cbz**). This feature is in accordance with the trend obtained by theoretical calculations (−5.18/−1.76 eV for **[4]C-Bu-Cbz** vs −5.19/−1.83 eV for **[5]C-Bu-Cbz**).

This HOMO/LUMO evolution with size is significantly less intense than that previously reported for cyclofluorenes (gap: 2.9/2.5 eV for cyclofluorenes with four and five units, respectively[25]), showing the key role played by the building unit on the molecular orbital energies in nanohoop chemistry. The influence of the bridge is also an interesting feature to determine. Bridging leads to an increase of the HOMO energy of 0.28 from −5.50 eV for **[10]CPP** to −5.22 eV for **[5]C-Bu-Cbz** but keeps the LUMO energies unaffected (−2.51 eV for both **[10]CPP** and **[5]C-Bu-Cbz**) giving a gap contraction of 0.29 eV. In the series with 8 phenyl units, **[8]CPP** and **[4]C-Bu-Cbz**, the opposite effect is observed: the LUMO is more affected by the bridge (−2.60 eV for **[8]CPP** vs −2.40 eV for **[4]C-Bu-Cbz**) than the HOMO (−5.28 eV for **[8]CPP** vs −5.18 eV for **[4]C-Bu-Cbz**) leading to decrease of the HOMO–LUMO gap (2.68 eV for **[8]CPP** vs 2.78 eV for **[4]C-Bu-Cbz**). At a first glance, it can be hypothesized that the presence of an electron rich atom such as nitrogen in cyclocarbazoles logically increases the HOMO energy level compared to their CPP analogues. However, in nanohoops, the distortion of the hoop induced by steric effects can also have an important impact on these energy levels.[48] The presence of one nitrogen bridge thus induces two effects: a steric effect (rigidification of two phenylene units) and an electronic effect (arising from the electron donating behaviour of the nitrogen) shifting both the HOMO/LUMO energy levels. In order to discriminate the electronic versus geometric impact of the bridges, we computed the HOMO and LUMO levels of **[8]CPP** and **[10]CPP** both in their optimized geometry and in the optimized geometry of **[4]C-Bu-Cbz** and **[5]C-Bu-Cbz**, in which the bridges have been removed and replaced by hydrogen atoms. For both sizes, we observed the same trend: the HOMO is more affected by the geometry (for **[10]CPP**, −5.45 and −5.23 eV in the optimized geometry and in the geometry of its bridged analogue respectively and for **[8]CPP**, −5.37 and −5.23 eV) than the LUMO (for **[10]CPP**, −2.20 and −2.26 eV in the optimized geometry and in the geometry of its bridged analogue respectively and for **[8]CPP**, −2.27 eV for both geometries). Thus, the increase of the HOMO upon bridging is predominantly due to the modification of the geometry of the nanohoop and the increase of the LUMO is due to the electron-donating nature of the nitrogen atom.

The optical properties of both **[4]C-Bu-Cbz** and **[5]C-Bu-Cbz** (Figure 2) and their corresponding CPP homologues (**[8]CPP** and **[10]CPP**) were characterized by UV/visible absorption spectroscopy as well as stationary and time-resolved emission spectroscopy in cyclohexane (Figures S17–S28). Both **[4]C-Bu-Cbz** and **[5]C-Bu-Cbz** display similar absorption spectra with the main bands and shoulders at 257/292/337/410 nm for **[4]C-Bu-Cbz** and at 265/292/342/410 nm for **[5]C-Bu-Cbz**, (Figure 2). One can note that the shoulder at 410 nm in **[5]C-Bu-Cbz** is more intense than that in **[4]C-Bu-Cbz**. TD-DFT analyses indicate that these shoulders and the lowest energy bands of both nanohoops are due to similar transitions involving similar orbitals (Figure 3). The shoulder above 400 nm is classically assigned, in the case of **[4]C-Bu-Cbz**, to a symmetry forbidden HOMO→LUMO transition (oscillator strength equal to 0.000). However, in **[5]C-Bu-Cbz**, due to the odd number of carbazole

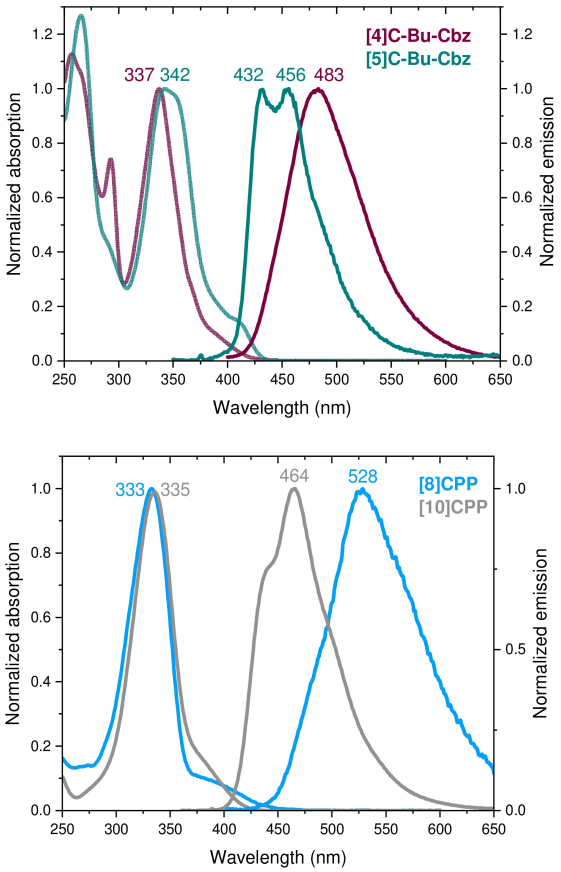

Figure 2. Absorption/emission spectra in cyclohexane of **[4]C-Bu-Cbz** and **[5]C-Bu-Cbz** (top: λ_{ex} = 337 and 340 nm for **[4]C-Bu-Cbz** and **[5]C-Bu-Cbz**, respectively) and **[8]CPP** and **[10]CPP** (bottom: λ_{ex} = 350 nm).

units and the resulting symmetry breaking, the oscillator strength is weak but not null (f = 0.08). This is the reason why the shoulder detected at around 400 nm is more intense for **[5]C-Bu-Cbz** compared to **[4]C-Bu-Cbz**.

One can also note that the main band of **[5]C-Bu-Cbz** centred at 342 nm is broader than that of **[4]C-Bu-Cbz** centred at 337 nm. This is also due to the lower symmetry of the nanohoop based on an odd number of carbazole units. While the orbitals of **[4]C-Bu-Cbz** are degenerate and optical transitions simulated at the same energy, the lower symmetry of **[5]C-Bu-Cbz** induces a larger number of transitions at different energies. This size dependence broadening is not observed for CPP analogues (Figures S27–S28), which are both based on an even number of phenylene units and are thus highly symmetrical. This shows the singularity of the optical properties of cyclocarbazoles versus those of CPP parents.

The emission spectrum of **[5]C-Bu-Cbz** in cyclohexane shows two maxima at 432 and 456 nm. This spectrum is structured in comparison with its smaller analogue **[4]C-Bu-Cbz** (only one band at 483 nm) and its unbridged analogue **[10]CPP** (which displays nevertheless a shoulder around 440 nm in addition to the band at 464 nm), Figure 2. This property is different from all cyclocarbazoles and CPPs (until 10 units) reported to date but similar to what is observed for cyclo-

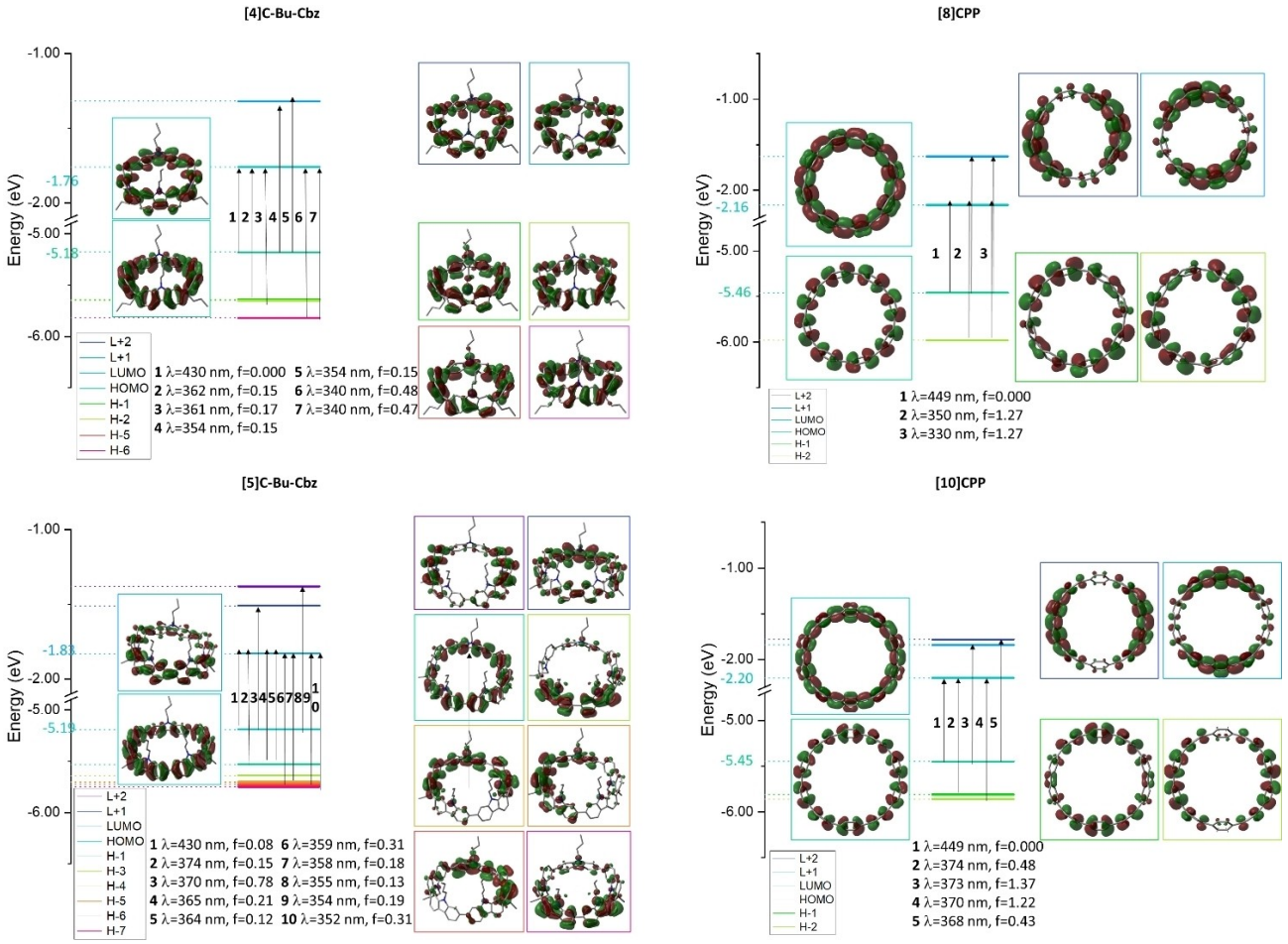

Figure 3. Representation of the energy levels and the main molecular orbitals involved in the electronic transitions of **[4]C-Bu-Cbz** and **[5]C-Bu-Cbz** (left) and **[8]CPP** and **[10]CPP** (right) obtained from TD-DFT, B3LYP/6–311 + G(d,p), shown with an isovalue of 0.02 [ebohr^{-3}]$^{1/2}$. For clarity, only the major contribution of each transition is shown (see the Supporting Information for details).

fluorenes with five units, analogues of **[5]C-Bu-Cbz** displaying also 10 phenylenes and five bridges (Figure S26).[25] Thus, the structured emission spectrum could be due to the planarization of a part of **[5]C-Bu-Cbz** in its excited state, facilitated by its larger size (compared to **[4]C-Bu-Cbz**) and the bridges (compared to **[10]CPP**). Furthermore, the fluorescence maximum of **[5]C-Bu-Cbz** is blue-shifted by 51 nm compared to **[4]C-Bu-Cbz** similarly to the trend observed for **[10]CPP** and **[8]CPP** (blue shift of 64 nm when the size increases). The fluorescence quantum yields of **[5]C-Bu-Cbz** and **[4]C-Bu-Cbz** are 0.56 and 0.20, respectively, close to those of **[10]CPP** and **[8]CPP**, 0.59 and 0.25, respectively. Thus, the bridges have an influence on the shape and width of the emission spectra but not on the fluorescence efficiency. This is an interesting consideration, which should be considered for the further design of high-efficiency emitters based on nanohoops. In addition, **[5]C-Bu-Cbz** displays a lifetime which is half the one of **[4]C-Bu-Cbz** (respectively 3.1 and 6.2 ns), similarly to what is observed for the CPP analogues (3.9 and 10.6 ns respectively for **[10]CPP** and **[8]CPP**). Thus, as for quantum yield, the lifetime of these nanohoops appears to be more affected by their size than by the presence of the bridges. The high quantum yields of the large nanohoops (ca. 0.6 for **[5]C-Bu-Cbz** and **[10]CPP**) is linked to the fact that their radiative constant k_r (181 and 151 μs^{-1}, respectively) are superior to their non-radiative constant k_{nr} (respectively 142 and 105 μs^{-1}) whereas the small nanohoops (**[4]C-Bu-Cbz** and **[8]CPP**) display a k_r (respectively 32.2 and 23.6 μs^{-1}) much lower than their k_{nr} (respectively 129 and 70.8 μs^{-1}). Therefore, as the strain energy increases, the quantum yield decreases. Note also that the k_{nr} of the bridged nanohoops are higher than those of the CPPs. This could be assigned to the dynamic of the alkyl chains, increasing non-radiative pathways.

In thin film, both absorption and emission spectra of **[4]C-Bu-Cbz** and **[5]C-Bu-Cbz** are similar to those in solution except that they are slightly red-shifted, indicating the absence of strong aggregation in the solid state (Figures S18 and S22). It should be noted that the quantum yields of **[4]C-Bu-Cbz** and **[5]C-Bu-Cbz** are almost equivalent in thin film (0.13 and 0.14%, respectively) whereas in solution the largest nanohoop displays the highest quantum yield (0.2 for **[4]C-Bu-Cbz** and 0.56 for

Table 1. Selected photophysical, electrochemical, theoretical and charge transport data of cyclocarbazoles and corresponding CPPs.

	[4]C-Bu-Cbz	[5]C-Bu-Cbz	[8]CPP	[10]CPP
Photophysics				
λ_{ABS}[a] [nm] sol	337	342	333	335
λ_{ABS}[a] [nm] film	347	359	346	351
λ_{EM}[a] [nm] sol	483	432, 456	528	464
λ_{EM}[a] [nm] film	495, 518	458	570	475
Φ[a] sol	0.20	0.56	0.25	0.59
Φ[a] film	0.13	0.14	0.08	0.34
τ_f[a] [ns]	6.2	3.1	10.6	3.9
k_r [μs^{-1}]	32.2	181	23.6	151
k_{nr} [μs^{-1}]	129	142	70.8	105
Electrochemistry				
HOMO[b] [eV]	−5.18	−5.22	−5.28	−5.50
LUMO[b] [eV]	−2.40	−2.51	−2.60	−2.51
ΔE_{EL} [eV]	2.78	2.71	2.68	2.99
Theoretical calculations				
HOMO[c] [eV]	−5.18	−5.19	−5.37	−5.45
LUMO[c] [eV]	−1.76	−1.83	−2.27	−2.20
ΔE_{TH} [eV]	3.42	3.36	3.10	3.25
Charge transport				
μ_{FElin} [$\times 10^{-5}$ $cm^2V^{-1}s^{-1}$]	1.03	0.93	d	d
μ_{FEsat} [$\times 10^{-5}$ $cm^2V^{-1}s^{-1}$]	1.04	4.22	d	d
V_{TH} [V]	−12.8	−28.8	d	d
SS [V/Dec]	0.89	4.4	d	d
μ_{SCLC} [$\times 10^{-4}$ $cm^2V^{-1}s^{-1}$][e]	2.78	0.78	0.00121	0.00011

[a] in cyclohexane, [b] from CVs recorded in CH_2Cl_2 for oxidation and in DMF for reduction, [c] from B3LYP/6–311+G(d,p), [d] non measurable, [e] from SCLC.

[5]C-Bu-Cbz). Thus, the size of the cyclocarbazole does not impact its emission efficiency in the solid state.

Finally, OFET electrical characterizations and I–V measurements in two-terminal devices were performed to investigate the charge transport properties of the different nanohoops (Table 1, Figure 5, below). The mobilities of **[10]CPP** and **[5]C-Bu-Cbz** are measured for the first time, whereas that of **[8]CPP** and **[4]C-Bu-Cbz** have been previously reported.[18] First, the nanohoops have been incorporated as active layer in OFETs possessing a bottom-gate bottom-contact (BG-BC) architecture (Figure S29[50,51]).

The first striking result is obtained with **[10]CPP** as no field effect mobility (μ_{FE}) is measured for this molecule. The same behaviour was observed for **[8]CPP**.[18] Theoretical calculations yield electronic couplings for holes between adjacent molecules (Figure 4) in the bulk crystal structure of **[10]CPP** (2 and 9 meV) slightly lower than in **[8]CPP** (10 and 18 meV); in contrast, the reorganization energy of **[10]CPP** is significantly lower than in **[8]CPP** (251 vs 313 meV). The fact that the transfer integrals are much smaller than the reorganization energies indicate that charge transport operates in the hopping regime. Based on the Marcus expression of the hopping rate, see Equation (1) below, this further suggests that **[10]CPP** and **[8]CPP** should exhibit comparable hole mobilities. Taking the largest value of the transfer integrals and the corresponding reorganization energies, the ratio of k_{ET}-**[8]CPP**/k_{ET}-**[10]CPP** obtained from Equation (1) is indeed only on the order of 1.9.

$$k_{ET} = \frac{2\pi|J_{AB}|^2}{\hbar\sqrt{4\pi\lambda k_B T}} e^{-\frac{(\Delta G^0+\lambda)^2}{4\lambda k_B T}} \quad (1)$$

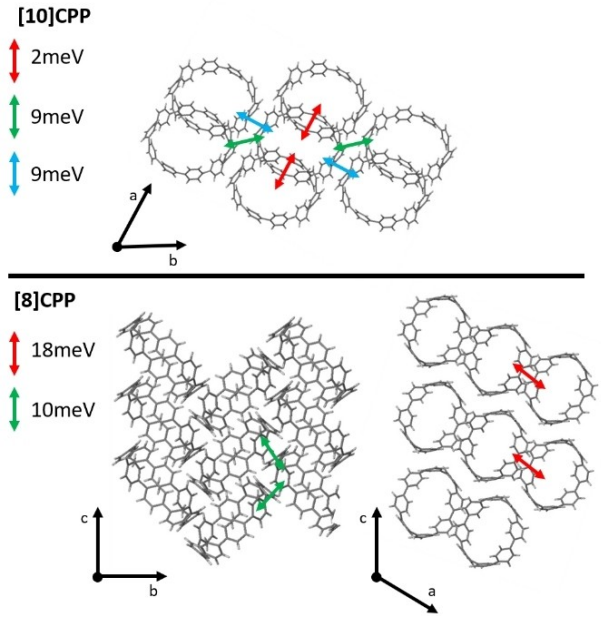

Figure 4. Computed electronic couplings for holes in the experimental crystal structure of **[10]CPP** (Top) and **[8]CPP** (bottom).

where k_{ET} is the hopping probability, J the electronic coupling, ΔG^0 the site energy difference between the two molecules (due here to the application of an external electric field) and λ the reorganization energy.

Cyclocarbazoles **[4]C-Bu-Cbz** and **[5]C-Bu-Cbz** display FE mobilities (Figure 5). As their HOMOs are higher than those of their CPP analogues, charge injection is favoured. The first

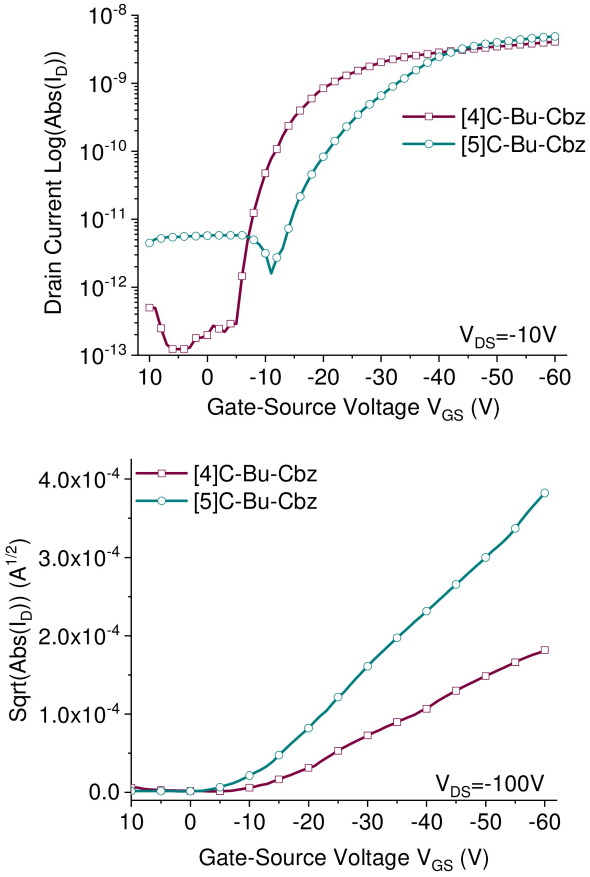

Figure 5. Transfer characteristics in linear (top) and saturated (bottom) regimes of **[4]C-Bu-Cbz** and **[5]C-Bu-Cbz**.

observation concerns the mobility in the saturated regime μ_{FEsat} ($V_{DS}=100$ V). Remarkably, **[5]C-Bu-Cbz** displays an μ_{FEsat} four times larger than that of its smaller analogue **[4]C-Bu-Cbz** (4.22×10^{-5} vs 1.04×10^{-5} $cm^2V^{-1}s^{-1}$, respectively). Thus, when the size of the hoop increases, μ_{FEsat} increases as well. As no μ_{FE} can be measured for both **[8]CPP** and **[10]CPP**, this finding also shows the importance of the nature of the building unit in the charge injection and/or transport properties. However, the saturated μ_{FEsat} are measured at high electric field, $V_{DS}=100$ V; in these conditions, traps into the semiconductor are filled and do not impact the carrier mobility. To compare the effect of the size, the capability of the nanohoop to accumulate charges at the interface with the insulator should also be considered, as reflected by the threshold voltage (V_{TH}) and subthreshold slope (SS). V_{TH} is the gate-source voltage needed for the channel to be populated while SS is the voltage required to increase the current at the semiconductor/insulator interface by one order of magnitude. SS is particularly important in that purpose as it depends on both the defect density at the insulator/semiconductor interface and on the chemical structure of the semiconductor itself. Indeed, if the density of traps is high, most of the carriers initially injected do not participate in the electrical conduction within the channel. SS reflects hence the organization of the layer. The lowest and thus the best SS is measured for **[4]C-Bu-Cbz**, 0.89 V/dec, whereas **[5]C-Bu-Cbz** displays a SS of 4.4 V/dec. The extraction of V_{TH} also confirms this trend since the lowest V_{TH} is estimated for the small nanohoop **[4]C-Bu-Cbz** ($V_{TH}=-12.8$ V) compared to the large one **[5]C-Bu-Cbz** ($V_{TH}=-28.8$ V). These data suggest that a small nanohoop is beneficial for a good organization of the molecules in thin films whereas a large one increases the density of structural defects, and hence of traps for the charge carriers, increasing in turn the V_{TH}.

To confirm this feature, AFM studies have been performed on the OFET layers (Figure 6). The film surface of both cyclocarbazoles **[4]C-Bu-Cbz** and **[5]C-Bu-Cbz**, deposited on SU-8 insulating layers, remarkably presents a regular and smooth morphology with low surface roughness (root mean roughness R_q respectively of 0.42 and 0.75 nm). One can nevertheless note that the R_q of **[4]C-Bu-Cbz** is lower than that of **[5]C-Bu-Cbz** in accordance with the SS and V_{TH} values presented above. These data are also in accordance with the differences observed between linear and saturated FE mobilities. For **[4]C-Bu-Cbz**, the linear FE mobility ($\mu_{FElin}=1.03\times10^{-5}$ $cm^2V^{-1}s^{-1}$) is almost identical to the saturated FE mobility ($\mu_{FEsat}=1.04\times10^{-5}$ $cm^2V^{-1}s^{-1}$); this indicates that the linear FE mobility is almost unaffected by traps. For **[5]C-Bu-Cbz**, we note a significant increase from 0.933×10^{-5} $cm^2V^{-1}s^{-1}$ for μ_{FElin} to 4.22×10^{-5} $cm^2V^{-1}s^{-1}$ for μ_{FEsat}, highlighting a higher trap density in **[5]C-Bu-Cbz** vs **[4]C-Bu-Cbz**. These data reflect the different degrees of molecular arrangements of the two cyclocarbazoles.

In order to further confirm this analysis, electrical stress, using the gate bias stress protocol, has been performed. A stretched exponential model has been applied to evaluate the structural trap effect on the electrical stability of OFETs (Figure 7).

From these measurements, three parameters have been extracted. The first, ΔV_{THmax}, is the maximum threshold voltage shift under unlimited stress, the second, β, is linked to the average deepness of level energy of traps and the third, t_0, corresponds to the time for a carrier to be trapped. Figure 7 shows clearly the difference of electrical stability between OFETs made with either **[4]C-Bu-Cbz** or **[5]C-Bu-Cbz**. Interestingly, the carriers are quickly trapped in the case of **[5]C-Bu-Cbz** ($t_0=1.4\times10^3$ s) in comparison with **[4]C-Bu-Cbz** ($t_0=3.9\times10^4$ s). The maximum threshold voltage shift is also higher for **[5]C-Bu-Cbz** ($\Delta V_{THmax}=30.3$ V) than for **[4]C-Bu-Cbz** ($\Delta V_{THmax}=23.3$ V). The energy level of traps into the **[5]C-Bu-Cbz** layer ($\beta=0.69$) is also deeper than for **[4]C-Bu-Cbz** ($\beta=0.38$). These parameters extracted from electrical stress thus confirm the effect of nanohoop size on the layer organization.

The case of CPP analogues is somewhat different as both display a high surface roughness, $R_q=3.67$ nm for **[8]CPP** and $R_q=1.22$ nm for **[10]CPP** (Figure 6, bottom). These differences between the two families of nanohoops might be at the origin, at least partially, of the very different performance observed when incorporated in OFET devices.

The carrier mobilities were also extracted in a two-terminal device by applying the Mott–Gurney model to the I–V measurements (space-charge-limited current SCLC transport; Fig-

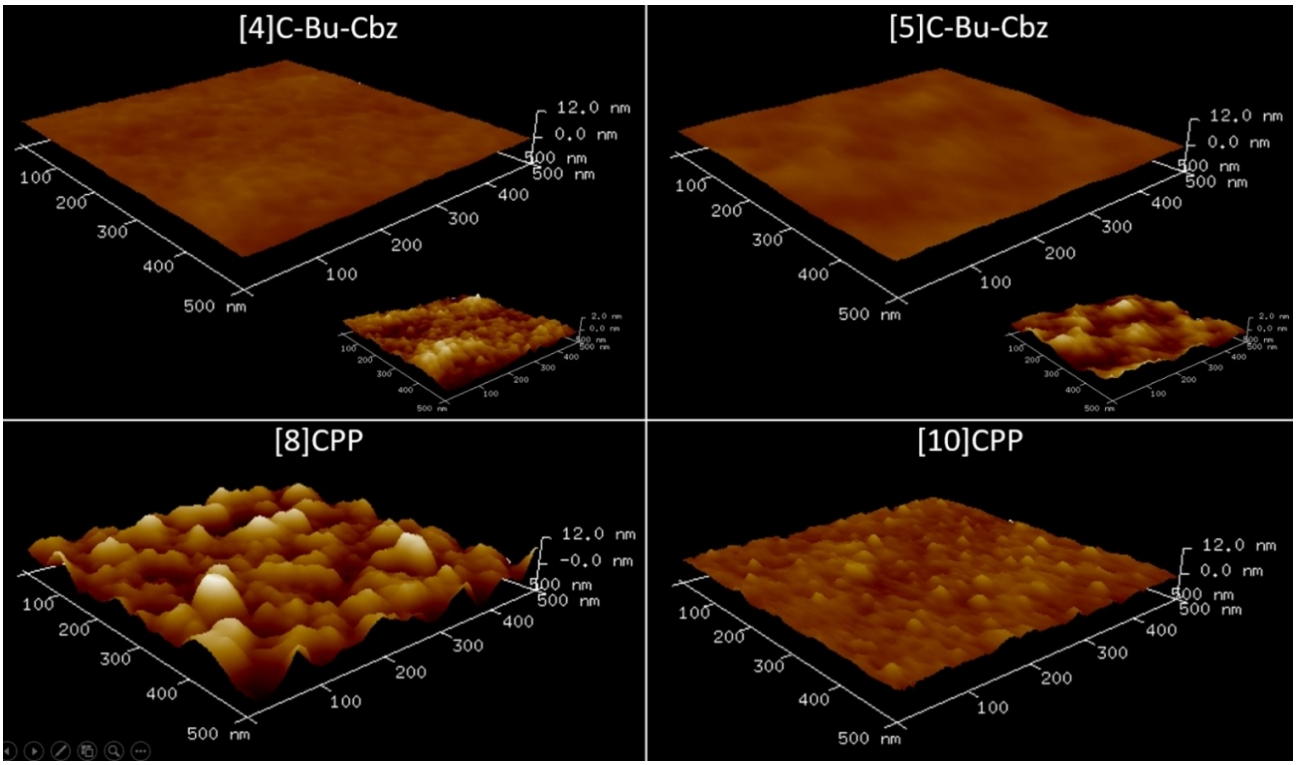

Figure 6. Two-dimensional (500×500 nm^2) AFM images of the semiconducting layer deposited under vacuum on an SU8 insulating layer.

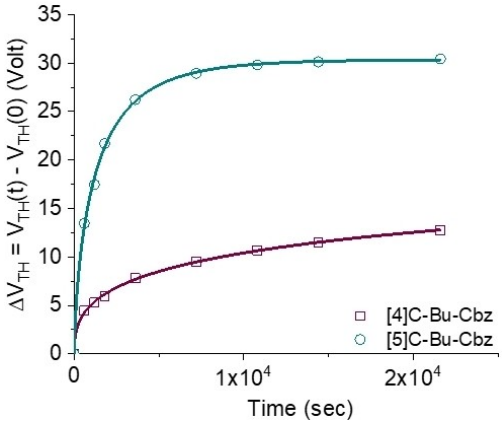

Figure 7. Threshold voltage behaviour under gate bias stress ($V_{GSstress} = -40$ V, $V_{DSstress} = -10$ V) for 6 h for **[4]C-Bu-Cbz** and **[5]C-Bu-Cbz**.

ure S30). The SCLC mobilities measured for the two cyclocarbazoles are about three orders of magnitude higher than those of their CPP analogues, showing the significant impact of the bridging on the charge transport properties (0.78/2.78×10^{-4} for the cyclocarbazoles vs 1.21/0.11×10^{-7} cm^{2}V^{-1}s^{-1} for the CPPs). This can be related to the significant differences observed in the AFM images between the two families of compounds (Figure 6). Note that for **[5]C-Bu-Cbz**, the electric field to be applied to fill the defects is higher than that of **[4]C-Bu-Cbz**, in accordance with the difference observed for μ_{FEsat}.

Thus, for both nanohoop families, when the size decreases, the charge carrier mobility increases (2.78×10^{-4} cm^{2}V^{-1}s^{-1} for **[4]C-Bu-Cbz** vs 7.75×10^{-5} cm^{2}V^{-1}s^{-1} for **[5]C-Bu-Cbz** and 1.21×10^{-7} cm^{2}V^{-1}s^{-1} for **[8]CPP** vs 1.1×10^{-8} cm^{2}V^{-1}s^{-1} for **[10]CPP**), showing how the nanohoop size can have important implications on the charge transport.

Unfortunately, the electronic couplings among the carbazole-based nanohoops cannot be computed in absence of crystalline structures. On the other hand, we can compute the second key parameter, that is, the internal reorganization energy (λreorg), in **[8]CPP**, **[10]CPP**, **[4]C-Bu-Cbz** and **[5]C-Bu-Cbz**, to understand how the nature of the building block and hoop size modify the geometric distortions in singly charged nanohoop. We considered the most stable isomer of **[5]C-Bu-Cbz** where carbazoles are in the order up/down/up/down/up. We have used a displaced harmonic oscillator model where we project each intramolecular normal mode of vibration on the vector describing the geometric changes between the neutral and charged state to partition the reorganization energies into mode contributions. The normal modes of vibration and their frequency were computed with the Gaussian package at the DFT level using the M062X functional curing for self-interaction issues[52] and a 6–31G(d,p) basis set (Figure 8). As the alkyl chains have no impact on the reorganization energies, they were replaced by hydrogen atoms. The normal mode contributions to relaxation energies were computed with the MOMAP package[53] that follows a previously reported methodology.[54] The DFT calculations yield the following total reorganization energies: **[8]CPP** (313 meV), **[10]CPP** (251 meV), **[4]C-Bu-Cbz**

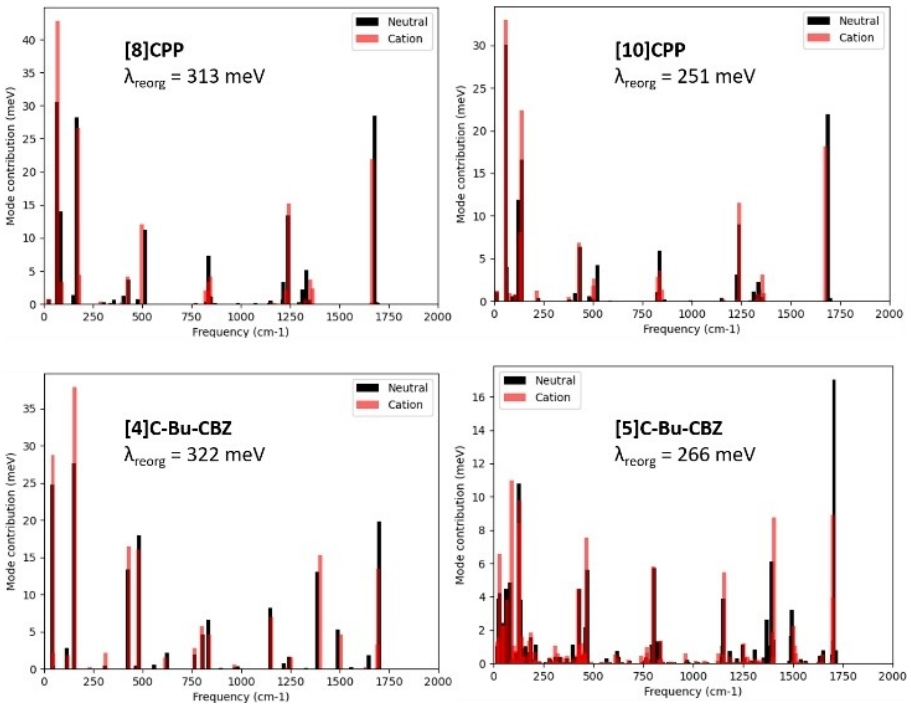

Figure 8. Relaxation energies on going from the neutral to oxidized geometry (red) and vice versa (black), partitioned into each mode contribution of a) **[8]CPP**, b) **[10]CPP**, c) **[4]C-Bu-Cbz** and d) **[5]C-Bu-Cbz** (the butyl chains have been removed for calculations). The total reorganization energy involved in the Marcus expression is the sum of the two contributions.

(322 meV) and **[5]C-Bu-Cbz** (266 meV). The results globally show that the number of carbazole units slightly increase the reorganization energy and conserve the dependency on the nanohoop size compared to the corresponding CPP analogues. Thus, as the size of the nanohoop increases, the reorganization energy decreases, as previously shown for CPPs by Houk, Yavuz and co-workers.[20] The significant decrease in the reorganization energy going from **[4]C-Bu-Cbz** to **[5]C-Bu-Cbz** is fully consistent with the larger FE mobilities measured in the staured regime; hopping rates estimated with Equation (1) for the same transfer integrals and the reorganization energies computed for **[4]C-Bu-Cbz** and **[5]C-Bu-Cbz** point to an increase by a factor of 2 with nanohoop size, in deep consistency with the factor of 4 measured experimentally in the OFET devices.

Looking into details in the contributors to the reorganization energies, we find a mode involving the dihedral torsions around 60 cm^{-1}, a second mode assigned to "nanohoop breathing" around 140 and 170 cm^{-1} for **[10]CPP** and **[8]CPP** respectively while the third mode is the notable C=C stretching of the benzene rings around 1670 cm^{-1}. Increasing the size of the nanohoop has lowered down the contributions of these modes by ~10 meV in **[10]CPP**. In the carbazole nanohoops, we do not recover such three dominating modes but more low to medium contributions to the reorganization energy with regard to the CPP molecules. In **[4]C-Bu-Cbz**, we observe the decrease in magnitude of the C=C contribution at 1670 cm^{-1}. A mode involving bending and torsion in the carbazole unit is also present at 40 cm^{-1}, and is comparable to the torsion modes present for the CPPs mentioned above. In the case of **[5]C-Bu-Cbz** compared to **[4]C-Bu-Cbz**, a higher number of low contributions to the relaxation energies arises when adding an extra carbazole unit. We do conserve a high contribution from the bending/torsion modes around 150 cm^{-1} and observe that the mode involving the benzene stretching has regained a sizeable contribution. These results demonstrate that geometry relaxation processes upon charging involve both changes in the geometry of the individual rings together with variations in the torsion angles between adjacent rings, thus promoting rather large internal reorganization energies. For the sake of comparison, the corresponding value is about 100 meV for a pentacene molecule made of five fused benzene rings.[55]

Conclusion

In the field of nanohoops, defining the evolution of the electronic properties as a function of the nanohoop size is a crucial step in the understanding of these new-generation π-conjugated systems and their applications, notably in organic electronics.[14,17,18,20,23] Thanks to the synthesis of the first cyclocarbazole with five building units, **[5]C-Bu-Cbz**, this work details the impact of the hoop size on the electronic and charge transport properties for two families of nanohoops, CPPs and cyclocarbazoles. The size expansion from four to five carbazole units leads to a decrease in both HOMO and LUMO energy levels providing a slight gap contraction of 0.08 eV. This gap contraction is less marked than that observed in cyclofluorenes series (0.4 eV), thereby showing the important role played by

the nature of the bridge in the tuning of molecular orbital energies. Regarding the optical properties, we show that the bridges have an influence on the shape, position and width of the emission spectra but not on the fluorescence efficiency.

The charge transport studies are the most important data reported herein considering the possible future of nanohoops in organic electronics. These studies correlate the nanohoop size to the mobility. We notably show that the saturated FE mobility of **[5]C-Bu-Cbz** is four times higher than that of its smaller analogue **[4]C-Bu-Cbz** (4.22×10^{-5} vs 1.04×10^{-5} $cm^2V^{-1}s^{-1}$). However, the study of V_{TH} and SS coupled to AFM studies suggests that a small nanohoop is more beneficial for a good organization of the molecules in thin films, whereas a larger nanohoop increases the density of structural defects, and hence of traps for the charge carriers. It is evident that other families of nanohoops and other nanohoop sizes should be investigated to go deeper into the establishment of design rules. Such studies are mandatory to reach high-performance devices based on nanohoops. In the light of recent works that have shown their potential in phosphorescent OLEDs,[23] nanohoops can become a new class of promising organic semiconductors.

Deposition Numbers 871414 (for **[8]CPP**) and 871415 (for **[10]CPP**) contain the supplementary crystallographic data for this paper. These data are provided free of charge by the joint Cambridge Crystallographic Data Centre and Fachinformationszentrum Karlsruhe Access Structures service.

Acknowledgements

This project received funding from the European Union's Horizon 2020 research and innovation program under grant agreement no. 699648 (FRODO). We thank GENCI (no. AD0100805032R1) for computing time, the ANR (no. 19-CE05-0024 and ANR-22-CE07-0041) for funding and for a post-doctoral fellowship (F.L.), the Region Bretagne (DIADEM project) and the ADEME (ECOELEC project) for PhD grants (F.L. and C.B., respectively), Nanorennes (Rennes) for access to clean-room facilities and CRMPO (Rennes) for mass analyses and variable temperatures NMR studies. We also thank Dr J. F. Bergamini for designing the graphical abstract. The work in Mons was supported by the Marie Curie ITN project UHMob (GA-811284) and the Consortium des Équipements de Calcul Intensif (CÉCI), funded by the Fonds de la Recherche Scientifique de Belgique (F.R.S.-FNRS) under grant # 2.5020.11. J.C. and D.B. are FNRS research directors.

Conflict of Interests

The authors declare no conflict of interest.

Data Availability Statement

Data available in article supplementary material.

Keywords: charge transport · cyclocarbazoles · hoop size effect · nanohoops

[1] S. R. Marder, J.-L. Bredas, *The WSPC Reference on Organic Electronics: Organic Semiconductors*, **2016**.
[2] Z.-Q. Jiang, C. Poriel, N. Leclerc, *Mater. Chem. Front.* **2020**, *4*, 2497–2498.
[3] K. Zhou, H. Dong, H.-L. Zhang, W. Hu, *Phys. Chem. Chem. Phys.* **2014**, *16*, 22448–22457.
[4] R. Ganesamoorthy, G. Sathiyan, P. Sakthivel, *Sol. Energy Mater. Sol. Cells* **2017**, *161*, 102–148.
[5] H. W. Kroto, *Angew. Chem. Int. Ed.* **1992**, *31*, 111–129.
[6] D. M. Guldi, B. M. Illescas, C. M. Atienza, M. Wielopolski, N. Martín, *Chem. Soc. Rev.* **2009**, *38*, 1587–1597.
[7] R. Jasti, J. Bhattacharjee, J. Neaton, C. R. Bertozzi, *J. Am. Chem. Soc.* **2008**, *130*, 17646–17647.
[8] H. Omachi, Y. Segawa, K. Itami, *Acc. Chem. Res.* **2012**, *45*, 1378–1389.
[9] E. R. Darzi, R. Jasti, *Chem. Soc. Rev.* **2015**, *44*, 6401–6410.
[10] M. R. Golder, R. Jasti, *Acc. Chem. Res.* **2015**, *48*, 557–566.
[11] S. E. Lewis, *Chem. Soc. Rev.* **2015**, *44*, 2221–2304.
[12] S. Yamago, E. Kayahara, T. Iwamoto, *Chem. Rec.* **2014**, *14*, 84–100.
[13] Y. Segawa, A. Kukazawa, S. Matsuura, H. Omachi, S. Yamaguchi, S. Irle, K. Itami, *Org. Biomol. Chem.* **2012**, *10*, 5979–5984.
[14] E. J. Leonhardt, R. Jasti, *Nat. Chem. Rev.* **2019**, *3*, 672–686.
[15] Y.-Y. Liu, J.-Y. Lin, Y.-F. Bo, L.-H. Xie, M.-D. Yi, X.-W. Zhang, H.-M. Zhang, T.-P. Loh, W. Huang, *Org. Lett.* **2016**, *18*, 172–175.
[16] E. Kayahara, L. Sun, H. Onishi, K. Suzuki, T. Fukushima, A. Sawada, H. Kaji, S. Yamago, *J. Am. Chem. Soc.* **2017**, *139*, 18480–18483.
[17] F. Lucas, L. Sicard, O. Jeannin, J. Rault-Berthelot, E. Jacques, C. Quinton, C. Poriel, *Chem. Eur. J.* **2019**, *25*, 7740–7748.
[18] F. Lucas, N. McIntosh, E. Jacques, C. Lebreton, B. Heinrich, B. Donnio, O. Jeannin, J. Rault-Berthelot, C. Quinton, J. Cornil, C. Poriel, *J. Am. Chem. Soc.* **2021**, *143*, 8804–8820.
[19] S. Wang, X. Li, K. Wei, X. Zhang, S. Yang, G. Zhuang, P. Du, *Eur. J. Org. Chem.* **2022**, *2022*, e202101493.
[20] J. B. Lin, E. R. Darzi, R. Jasti, I. Yavuz, K. N. Houk, *J. Am. Chem. Soc.* **2019**, *141*, 952–960.
[21] S. Canola, C. Graham, Á. J. Pérez-Jiménez, J.-C. Sancho-García, F. Negri, *Phys. Chem. Chem. Phys.* **2019**, *21*, 2057–2068.
[22] J. C. Sancho-García, M. Moral, A. J. Pérez-Jiménez, *J. Phys. Chem. C* **2016**, *120*, 9104–9111.
[23] C. Brouillac, F. Lucas, D. Tondelier, J. Rault-Berthelot, C. Lebreton, E. Jacques, C. Quinton, C. Poriel, *Adv. Opt. Mater.* **2022**, 2202191.
[24] V. Coropceanu, J. Cornil, D. A. da Silva Filho, Y. Olivier, R. Silbey, J. L. Brédas, *Chem. Rev.* **2007**, *107*, 926–952.
[25] L. Sicard, F. Lucas, O. Jeannin, P. A. Bouit, J. Rault-Berthelot, C. Quinton, C. Poriel, *Angew. Chem. Int. Ed.* **2020**, *59*, 11066–11072.
[26] G. Povie, Y. Segawa, T. Nishihara, Y. Miyauchi, K. Itami, *J. Am. Chem. Soc.* **2018**, *140*, 10054–10059.
[27] Z. Zhou, Z. Wei, T. A. Schaub, R. Jasti, M. A. Petrukhina, *Chem. Sci.* **2020**, *11*, 9395–9401.
[28] N. Grabicki, K. T. D. Nguyen, S. Weidner, O. Dumele, *Angew. Chem. Int. Ed. Engl.* **2021**, *60*, 14909–14914.
[29] J. S. Wössner, J. Kohn, D. Wassy, M. Hermann, S. Grimme, B. Esser, *Org. Lett.* **2022**, *24*, 983–988.
[30] J. S. Wössner, D. Wassy, A. Weber, M. Bovenkerk, M. Hermann, M. Schmidt, B. Esser, *J. Am. Chem. Soc.* **2021**, *143*, 12244–12252.
[31] K. Okada, A. Yagi, Y. Segawa, K. Itami, *Chem. Sci.* **2017**, *8*, 661–667.
[32] M. Fujitsuka, C. Lu, B. Zhuang, E. Kayahara, S. Yamago, T. Majima, *J. Phys. Chem. A* **2019**, *123*, 4737–4742.
[33] T. C. Lovell, C. E. Colwell, L. N. Zakharov, R. Jasti, *Chem. Sci.* **2019**, *10*, 3786–3790.
[34] A. C. Grimsdale, K. Müllen, *Macromol. Rapid Commun.* **2007**, *28*, 1676–1702.
[35] C. Poriel, J. Rault-Berthelot, *Acc. Chem. Res.* **2018**, *51*, 1818–1830.
[36] J.-D. Peltier, B. Heinrich, B. Donnio, O. A. Ibraikulov, T. Heiser, N. Leclerc, J. Rault-Berthelot, C. Poriel, *Mater. Chem. Front.* **2022**, *6*, 225–236.
[37] M. Romain, D. Tondelier, J.-C. Vanel, B. Geffroy, O. Jeannin, J. Rault-Berthelot, R. Métivier, C. Poriel, *Angew. Chem. Int. Ed.* **2013**, *52*, 14147–14151.
[38] C. Poriel, C. Quinton, F. Lucas, J. Rault-Berthelot, Z. Q. Jiang, O. Jeannin, *Adv. Funct. Mater.* **2021**, 2104980.
[39] F. Lucas, J. Rault-Berthelot, C. Quinton, C. Poriel, *J. Mater. Chem. C* **2022**, *10*, 14000–14009.

[40] S. Yamago, Y. Watanabe, T. Iwamoto, *Angew. Chem. Int. Ed.* **2010**, *49*, 757–759.
[41] H. Jia, Y. Gao, Q. Huang, S. Cui, P. Du, *Chem. Commun.* **2018**, *54*, 988–991.
[42] Z. Sun, T. Mio, K. Ikemoto, S. Sato, H. Isobe, *J. Org. Chem.* **2019**, *84*, 3500–3507.
[43] Z. Sun, K. Ikemoto, T. M. Fukunaga, T. Koretsune, R. Arita, S. Sato, H. Isobe, *Science* **2019**, *363*, 151–155.
[44] H.-W. Jiang, T. Tanaka, H. Mori, K. H. Park, D. Kim, A. Osuka, *J. Am. Chem. Soc.* **2015**, *137*, 2219–2222.
[45] Y. Kuroda, Y. Sakamoto, T. Suzuki, E. Kayahara, S. Yamago, *J. Org. Chem.* **2016**, *81*, 3356–3363.
[46] M. D. Peeks, T. D. Claridge, H. L. Anderson, *Nature* **2017**, *541*, 200–203.
[47] T. Iwamoto, Y. Watanabe, Y. Sakamoto, T. Suzuki, S. Yamago, *J. Am. Chem. Soc.* **2011**, *133*, 8354–8361.
[48] L. Sicard, O. Jeannin, J. Rault-Berthelot, C. Quinton, C. Poriel, *ChemPlusChem* **2018**, *83*, 874–880.
[49] E. Kayahara, R. Qu, M. Kojima, T. Iwamoto, T. Suzuki, S. Yamago, *Chem. Eur. J.* **2015**, *21*, 18939–18943.
[50] J.-D. Peltier, B. Heinrich, B. Donnio, O. Jeannin, J. Rault-Berthelot, E. Jacques, C. Poriel, *J. Mater. Chem. C* **2018**, *6*, 13197–13210.
[51] S. Bebiche, P. Cisneros-Perez, T. Mohammed-Brahim, M. Harnois, J. Rault-Berthelot, C. Poriel, E. Jacques, *Mater. Chem. Front.* **2018**, *2*, 1631–1641.
[52] Y. Zhao, D. G. Truhlar, *Theor. Chem. Acc.* **2008**, *120*, 215–241.
[53] Z. Shuai, *Chin. J. Chem.* **2020**, *38*, 1223–1232.
[54] J. R. Reimers, *J. Chem. Phys.* **2001**, *115*, 9103–9109.
[55] V. Coropceanu, M. Malagoli, D. A. da Silva Filho, N. E. Gruhn, T. G. Bill, J. L. Brédas, *Phys. Rev. Lett.* **2002**, *89*, 275503.

Manuscript received: March 24, 2023
Accepted manuscript online: March 30, 2023
Version of record online: June 1, 2023